AIAA JOURNAL
Vol. 30, No. 9, September 1992

Application of a Solution Adaptive Grid Scheme to Complex Three-Dimensional Flows

Carol B. Davies*
Sterling Software, Palo Alto, California 94303
and
Ethiraj Venkatapathy*
Eloret Institute, Sunnyvale, California 94087

A new three-dimensional adaptive grid code (SAGE) based on the algebraic, solution-adaptive scheme of Nakahashi and Deiwert has been developed and applied to a variety of problems. This report describes its application to a range of complex three-dimensional, supersonic, and hypersonic flows. Examples discussed are a tandem-slot fuel injector, the hypersonic forebody of the Aeroassist Flight Experiment, the three-dimensional base flow behind the Aeroassist Flight Experiment, the supersonic flow around a three-dimensional swept ramp, and a generic, hypersonic, three-dimensional nozzle-plume flow. The associated adapted grids and the solution enhancements resulting from a grid adaption are presented for each case.

Introduction

SOLUTION-adaptive grid methods have become an important tool for accurately computing both simple and complex flows in two and three dimensions. Grid adaption procedures in general either redistribute points or refine distribution (by adding points), thus reducing solution errors by minimizing grid discretization errors. This minimization problem has been well formulated by Brackbill and Saltzman[1] for grid redistribution schemes and by Berger and Oliger[2] and Dannenhoffer and Baron[3] for grid refinement schemes. A good review of the multitude of adaptive grid schemes can be found in Ref. 4.

The approach taken here is based on grid point redistribution through local error minimization. Gnoffo[5] first introduced a method for the redistribution of grid points based on local flow gradients. This method is analogous to finding the equilibrium position of a system of springs that connect each node with adjacent nodes and whose spring force (or tension constant) is proportional to the local error or weight function. The spring analogy, with the proper choice of weight function, results in a simple system of algebraic equations in a one-dimensional tridiagonal form. Nakahashi and Deiwert extended this method to higher dimensions.[6-8] In two and three dimensions, the resulting system of equations can be approximated by a series of one-dimensional spring-analogy problems. Nakahashi and Deiwert formulated an appropriate weight function that not only was proportional to local flow gradients but that also allowed grid control by user-specified minimum and maximum grid spacing. Since the multidimensional problem was posed as a series of one-dimensional problems, the associated adapted grid was not smooth between the adapted lines. Nakahashi and Deiwert therefore introduced grid-smoothing functions between the lines that are analogous to torsion springs. This procedure was found to be efficient and fast and it allowed the user to control the quality of the grid while performing the solution adaption.

The present method has been explored extensively and applied to a variety of flows.[8-13] A user-friendly computed code called self-adaptive grid code (SAGE), with many enhancements, was previously developed for two-dimensional and axisymmetric flow problems.[9] References 8, 9, and 12 show various flow problems for which the two-dimensional version of the code has been successfully used. This code has been distributed nationwide and is available through COSMIC. Its extensive use by the computational fluid dynamics (CFD) community prompted us to extend it to three dimensions and explore the complexities in three-dimensional flow problems. Though Nakahashi and Deiwert[6-8] extended their two-dimensional procedure to three dimensions, and this was followed by a further use of the scheme by Djomehri and Deiwert,[14] experience in applying this scheme to three-dimensional problems has been limited. In addition, since the SAGE code is capable of adapting multiple zonal grids, overlapping grids, C-type, H-type, and O-type grids with periodic boundaries, and overlapping grids with holes, the extension of this code to three dimensions allows us to explore a wide variety of three-dimensional problems using the flexibility already demonstrated in the two-dimensional version.

The present paper describes the results that clearly demonstrate the usefulness of the three-dimensional adaptive grid

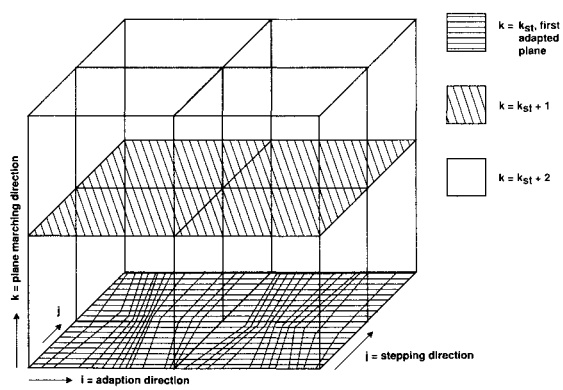

Fig. 1 Relationship of adaption planes.

Presented as Paper 91-1594 at the AIAA 10th Computational Dynamics Conference, Honolulu, HI, June 24-27, 1991; received Aug. 2, 1991; revision received Jan. 6, 1992; accepted for publication Jan. 30, 1992.

*Consultant, NASA Ames Research Center, MS 230-2, Moffett Field, CA 94035. Member AIAA.

scheme. The grid smoothness requirements and adaptive requirements in three dimensions can be complex. Flow structures such as shocks and supersonic shear layers are captured more accurately when the grid is aligned with the flow structure. The grid alignment, orthogonality, and smoothness requirements are often found to be inconsistent with adaption if the adaption is carried out in all directions. However, limiting the adaption process to a local primary direction can still produce greatly improved flowfield solutions, as shown in the results.

Three-Dimensional Formulation

As stated in the Introduction, the three-dimensional adaption takes place as a series of one-dimensional adaptions. Figure 1 illustrates this concept; a flowfield solution has been obtained on the three computational planes shown, and the points on this grid are now being adapted to this flow solution. The first adaption occurs on the lower plane (k_{st}) along line j_{st} and then marches in the increasing j direction. The figure shows that points have already been redistributed along each j line on the k_{st} plane. The adaption then steps to the second plane (k_{st} + 1) with marching taking place in the same j direction. The stepping in k planes will continue until all planes have been adapted. For multidimensional adaption, it is possible to return and perform subsequent passes, adapting on top of the already adapted planes but marching in the alternate directions. This is an arbitrary order of adaption and marching directions; any sequence is allowed. The application of tension and torsion springs is illustrated in Fig. 2, which shows a segment of the grid with the current adaption line j on the upper plane, highlighting the tension spring constant ω_i that acts between each pair of nodes. Also shown are the torsion spring parameters: τ controls the smoothness within the plane, and ψ acts to control smoothness between planes. Thus, for each node (i, j, k) four forces control the redistribution of the point: ω_i, ω_{i-1}, τ_i, and ψ_i. The equation controlling the redistribution of points along each line thus consists of two parts: 1) the one-dimensional approach using tension spring constants, and 2) the torsion terms. The tension spring constants have the effect of clustering the redistributed points into the high-gradient regions. The torsion terms provide a correction to this redistribution to maintain continuity between sequentially adapted lines and planes.

A complete description of the development of the three-dimensional equations, including the definition of the torsion and tension terms, is given by the current authors in Ref. 15. Also included in Ref. 15 is a discussion on the enforcement of boundary conditions, an important feature that enhances the capabilities of the SAGE code.

Three-Dimensional Adaption

A few of the important questions in three-dimensional adaption are the choices of stepping and marching directions and the number of adaption passes to make. The answers will depend in large part on how the initial grid is aligned with respect to the flow structures. For two-dimensional adaption, four choices of stepping direction are available: stepping in the i direction, the j direction, or both (in either order). Each of these options will produce a different adapted grid. However, there is no way to quantify which of these will produce the best grid. It has been show that, for many applications, limiting the adaption to only one direction can produce adequately adapted grids.[9,13] The choice of this direction depends on the flow features and is often obvious to the user. For problems with multidirectional flow features, experimenting with the second adaption will determine if two passes are necessary and in which order they should be made. Two-directional adaptions can produce large local errors, as well as complicated and highly nonorthogonal (i.e., sheared) grid structures that may cause problems when restarting the flowfield code.

For three-dimensional adaption, the choice of stepping direction expands to two directions in each of the three planes, and since flow structures are more complex, the apparent need for two- or even three-directional adaption increases. However, even a one-directional adaption will significantly change the grid in all three directions, as shown in the following example. The problem shown in Fig. 3 is the University of Virginia combustor-flow experimental test.[16] Figure 3a shows a Mach 2 flow over a backward-facing step, with two sonic transverse air jets behind the step. An outline of the grid used for this adaption example is shown in the figure by dotted lines. The flow data (computed using the USA code under an

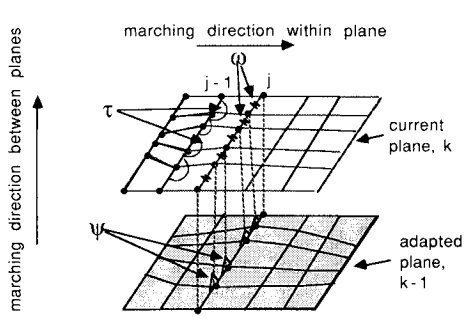

Fig. 2 Tension springs ω and torsion springs τ and ψ.

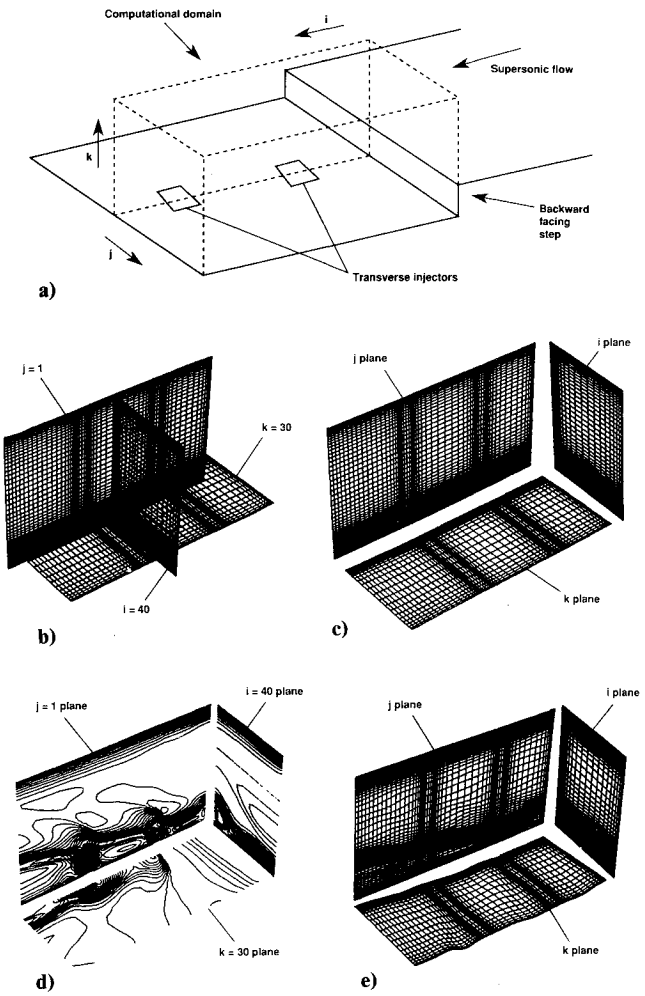

Fig. 3 Staged transverse injectors in a supersonic combustor: a) computational grid; b) three planes from the initial grid; c) same three planes, separated; d) Mach contours on initial grid; e) grid adaption based on Mach number, marching in j planes and stepping in the i direction within planes.

IR&D program) was provided by Jong H. Wang of Rockwell International. Figure 3b shows three selected planes, *i, j, k* from the initial grid; they are separated for clarity in Fig. 3c. Figure 3d shows the corresponding Mach contours from the initial flowfield solution that was used as the adaption variable. Adaption takes place on constant *j* planes with marching in the *i* direction within the plane. This implies that the points were redistributed along *k* lines. Figure 3e shows the adapted planes, and although only one adaption pass has been made, both the *i* and *j* planes are adapted with respect to Mach number, with the planes retaining their original three-dimensional surfaces. However, the *k* plane shows a different effect; points have not moved within the plane, but the three-dimensional surface has changed, since points have shifted in the *k* direction through the adaption.

It is fairly clear by looking at the constant *j* plane in Fig. 3e that a second adaption would be appropriate, by adapting in the *i* direction and stepping in *k* lines. Figure 4a shows the result of performing this adaption on top of the adaption already shown in Fig. 3e; points have now been redistributed in the *i* direction as well as the *k* direction. However, it should be noted that *i* redistribution can also occur by marching in *j* within the constant *k* planes. This adapted grid is seen in Fig. 4b and shows a very similar redistribution on the *j* plane, even though that was not the adaption plane. Several other combinations of marching and stepping directions were also tested, giving similar results. This indicates that the choice of adaption order may not be crucial to the creation of an acceptable adapted grid. In addition, it shows that two-directional adaptions can produce an adapted grid that sufficiently represents the complex three-dimensional flow features.

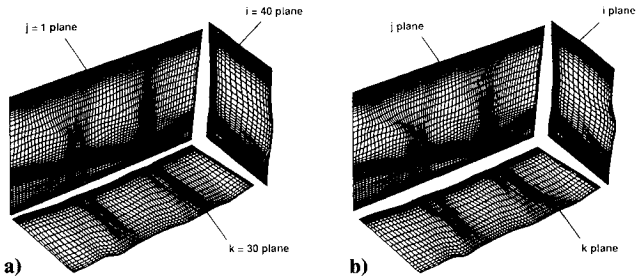

Fig. 4 Two-directional adaption: a) adapted grid obtained by marching in *j* planes and stepping in the *k* direction within planes, using the grid from Fig. 3e as the initial grid; b) adapted grid obtained by marching in *k* planes and stepping in the *j* direction within planes.

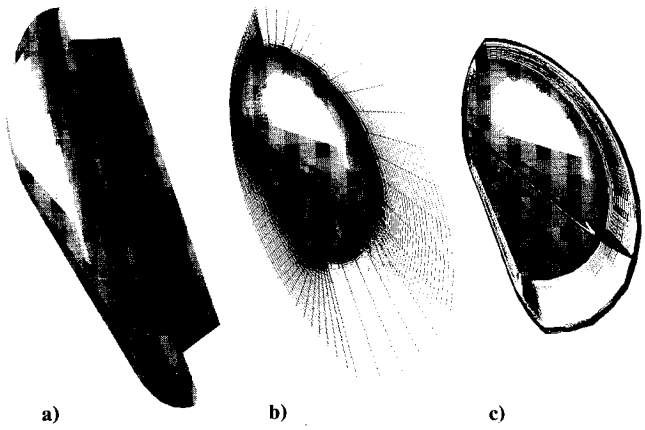

Fig. 5 AFE forebody flow: a) side view of vehicle geometry; b) nonadapted grid around the forebody; c) pressure contours computed on the initial grid.

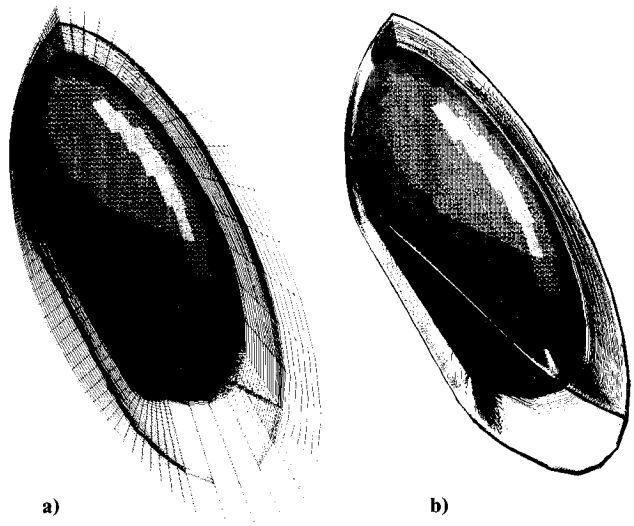

Fig. 6 AFE forebody flow: a) adapted grid; b) pressure contours computed on adapted grid.

Application of SAGE

Aeroassist Flight Experiment Forebody, Hypersonic, Nonequilibrium Flow

The first demonstration of the three-dimensional SAGE adaptive grid code is its application to the hypersonic, nonequilibrium flow around the forebody of the Aeroassist Flight Experiment (AFE) vehicle. The AFE is a full-scale experimental program whose purpose is to obtain flight data for a sufficiently large model on which the fluid, thermal, and chemical scales are matched to Aeroassisted Space Transfer Vehicles (ASTVs). These vehicles will be used in the future to transport materials and humans from high Earth orbit to low Earth orbit or in the moon and Mars environments. The AFE flight data will be used to validate CFD codes, and in turn, the CFD codes will be used to design future ASTVs. CFD codes are currently being used to predict both the forebody flow and the base flow around the AFE geometry under flight conditions at high altitudes. Some of the computational results obtained by Palmer[17,18] and Gnoffo[19] for the forebody are being used in the instrument design.

The critical feature around the forebody of the AFE is the three-dimensional blunt-body shock. Under flight conditions, the flowfield will be in a state of high nonequilibrium (both thermal and chemical).[18,19] Since most of the nonequilibrium flow solvers are of a shock-capturing type, the accuracy of the solution behind the shock (which controls the chemical and thermal nonequilibrium processes, which in turn govern the radiation from the shock layer) depends critically on the grid. Thus, selecting the proper grid structure becomes a very important constraint in accurately predicting the flow.

The AFE geometry and an initial grid around the vehicle forebody are shown in Figs. 5a and 5b. The solution computed on this nonadapted grid by the thermochemical nonequilibrium solver of Palmer[17,18] is shown in Fig. 5c. This three-dimensional nonequilibrium solver required approximately 64 h of CRAY-2 CPU time to compute on a $85 \times 23 \times 85$ grid. A grid refinement procedure to add points in the shock region would require an unacceptable amount of computer time to obtain a new solution. As a result, the grid redistribution method of SAGE was applied to the solution on the grid shown in Fig. 5b. The grid adaption was based on the pressure gradients across the shock. Because of the smooth shape of the shock, only the family of lines from the body to the outer boundary were adapted, and no additional adaptions in the other coordinate directions were necessary. The resulting adapted grid is shown in Fig. 6a. This grid was input to the flowfield code, and the newly computed pressure contours are shown in Fig. 6b. These three-dimensional contours show only

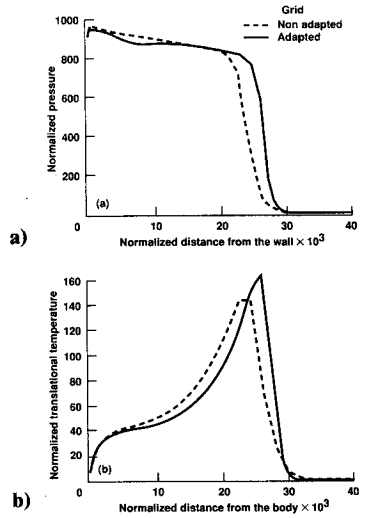

Fig. 7 Comparison of nonadapted and adapted results along the stagnation line: a) pressure; b) normalized translational temperature.

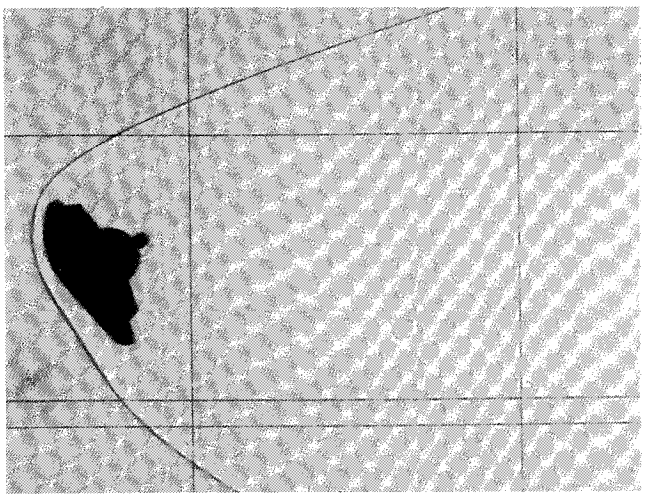

Fig. 8 Shadowgraph of the AFE hypersonic wake flow (side view) taken at NASA Ames Research Center, Hypersonic Free-Flight Facility.

the qualitative improvement to the solution. A comparison between the adapted and the nonadapted solutions in terms of pressure and translational temperature along the stagnation line is shown in Fig. 7. The steepening of the shock can be seen from the pressure comparison in Fig. 7a. Figure 7b compares translational temperatures, which are sensitive to the accuracy of the captured shock, and considerable improvement resulting from grid adaption is indicated. This is significant for the radiation and chemical species predictions.

Aeroassist Flight Experiment Base Flow

The base flow behind the AFE geometry is more complicated fluid dynamically than the forebody flowfield because of the viscous-inviscid interaction. Some of the prominent features in the base flow are the converging shear layer, the large recirculation zone, the development of the neck region, and the formation of the recompression shock. A sample shadowgraph shown in Fig. 8 was obtained at the Hypersonic Free-Flight Facility at NASA Ames Research Center and shows the development of the neck region and the recompression shock. Computations performed by Palmer,[18] Gnoffo,[19] and Tam and Li[20] do not show these significant flow structures in the wake. (However, it should be noted that none of these computations were performed to look critically at the base flow region.) The temperature contours from Ref. 17 that are drawn in Fig. 9 show the lack of resolution in the base region that prevents the base flow from developing. The base flow radiometer design requires more accurate flowfield and radiation-field predictions in the wake. To obtain better results, the SAGE code was used to adapt the grid. First the base flow grid used by Palmer in Ref. 18 was extended from one body diameter to five body diameters in the base region. The initial solution used in adapting the grid was obtained from a second-order-accurate chemically frozen formulation in the base region.[21] The adaption function was based on a combination of pressure, temperature, and density gradients, and the final adapted grid is shown in Fig. 10a. A solution was then obtained on the adapted grid and is shown in Fig. 10b in terms of temperature contours. The adapted solution was able to capture all of the expected flow structures in the wake. The qualitative comparison of the base flow with experimental shadowgraphs is found to be good, though a quantitative comparison is inappropriate because the conditions between the two differ significantly.

The final adapted grid shown in Fig. 10a was obtained in stages. First the outer bow shock was resolved by adapting the grid based on pressure gradients and computing a new flow solution. The grid was then readapted to the shear layer, this time using a combination of temperature and density gradients as the adaption variable. Once the shear layer was captured

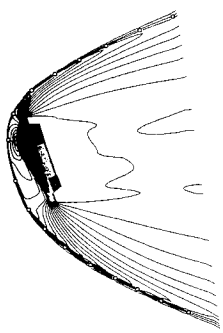

Fig. 9 AFE translational temperature contours from Palmer.[17]

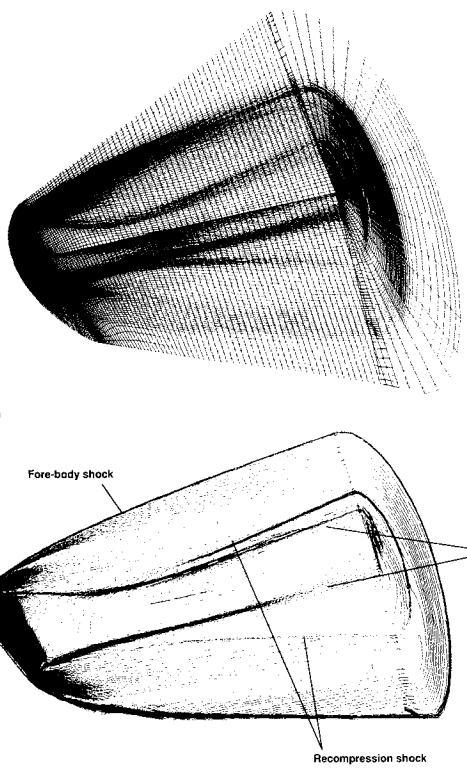

Fig. 10 AFE base flow: a) adapted grid; b) temperature contours.

with reasonable accuracy, the grids were readapted to the recompression shock. Since the evolution of the recompression shock depended on accurate shear-layer development, the multistage approach was necessary. As in the case of the forebody adaption, it was sufficient to adapt only on one set of coordinate lines.

Supersonic Flow over a Three-Dimensional Swept Ramp

Solutions were obtained and reported in Ref. 22 for supersonic flow over two three-dimensional swept ramps, one with sweep angle $\beta = 15$ deg and the other with $\beta = 30$ deg. The latter is shown in Fig. 11a. Oil flow patterns from experimental results[21] are shown in Fig. 11b for the 30-deg case, and the separation and reattachment regions are clearly marked. The recompression at the three-dimensional ramp corner region and the viscous-inviscid interaction with the boundary layer result in the large separation that is three dimensional in nature. Oil flow patterns from the 30-deg computed solution[22] are presented in Fig. 12a. For the 15-deg-ramp-angle case (not shown), the experimental and the numerical results agree well; however, for the 30-deg case, it can be seen that a significant difference exists in the size of the separation zone. This was suspected to be caused by local grid inaccuracies. Grid adaption was thus used, adapting to a combination of density, pressure, and Mach contours.

As in the previous example, grid adaption was performed in stages and, in addition, more grid points were added in the streamwise and normal (to the wall) directions. Figure 13a shows the initial grid used in the computations described in Ref. 21, and Fig. 13b shows the adapted grid. This new grid was able to capture more accurately the interaction between the shocks from the separated region and from the wall boundary layer. This improved interaction generated a larger separation zone than before, which is seen in the recomputed oil-flow patterns shown in Fig. 12b. This example demonstrates that a single-directional adaption influences the entire three-dimensional flow solution. The ramp surface plane was not adapted directly but, nevertheless, the flow on this surface changed considerably. The difference that still exists in the size of the separation zone is believed to be due to the approximate side-edge boundary conditions used in the numerical computations; the interaction between the lower part of the experimental geometry and the ramp (which is of interest here) was neglected, and the boundary conditions close to the side edge were approximated by simple extrapolation.

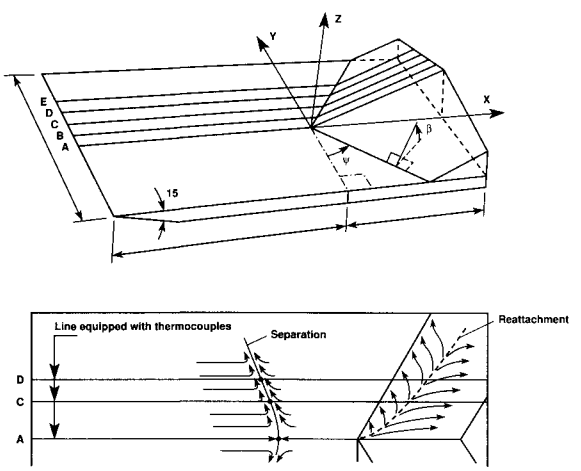

Fig. 11 Three-dimensional swept ramp: a) experimental model, with $\beta = 30$ deg; b) experimental oil-flow pattern on ramp surface, showing separation and reattachment regions.

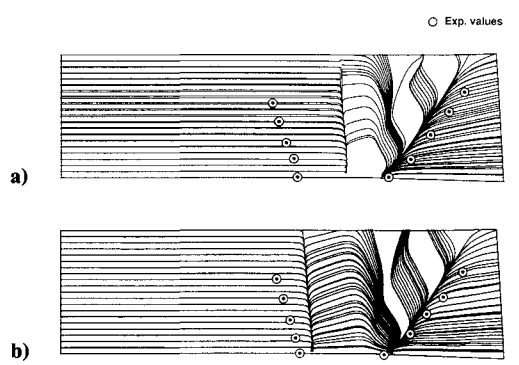

Fig. 12 Three-dimensional swept-ramp oil-flow patterns from computed solutions: a) from initial grid; b) from adapted grid.

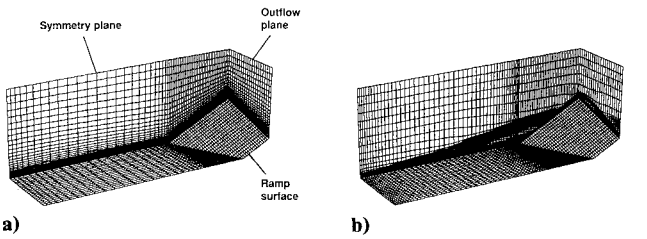

Fig. 13 Three-dimensional swept ramp: a) initial grid; b) adapted grid, using a combination of density, pressure, and Mach number as adaption variable.

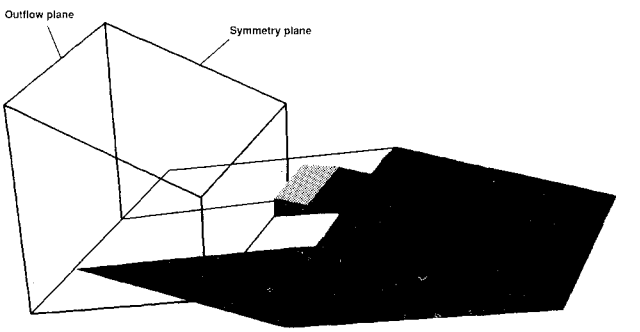

Fig. 14 SERN experimental model and the computational zone in the plume region.

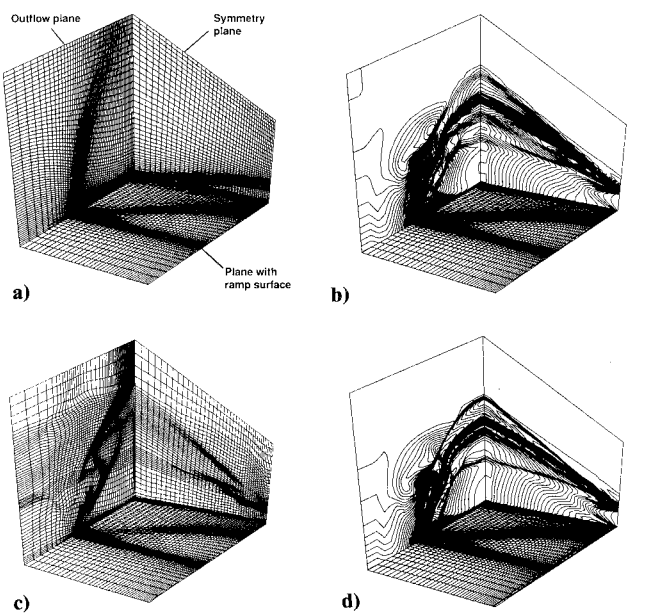

Fig. 15 Nozzle plume flow: a) initial grid showing symmetry plane, outflow plane, and ramp surface; b) initial Mach contours; c) adapted grid; d) Mach contours using adapted grid.

Hypersonic National Aero-Space Plane Nozzle-Plume Flow

Ideal gas solutions have been obtained with a multiple, three-dimensional grid topology for the supersonic flow around a generic National Aero-Space Plane (NASP) nozzle configuration known as the single exhaust ramp nozzle (SERN).[23] The three-dimensional model is shown in Fig. 14 along with an outline of the computational zone in the plume region. This grid is one of the eight separate overlapping grids that were required to model this problem. The interaction of the external flow with the nozzle-plume flow is much more complicated than the previous problems, and grid adaption for this case demonstrates the flexibility of using SAGE for adapting segments of multiple grids. Figure 15a shows three planes (the symmetry plane, the outflow plane, and the plane containing the ramp surface) from the original grid that covered the plume region. Figure 15b shows the Mach contours from the flowfield solutions obtained on this grid. Although most of the flow features were observed, they were not all well defined, and it was difficult to separate the features clearly. The initial grid was adapted in two stages: first the points were redistributed in two directions, based on Mach number; then points were moved from the outer, constant region to the more complex interior flow region.

The resulting adapted grid is shown in Fig. 15c. The inflow plane (not shown) and the lower ramp plane were not adapted to maintain continuity between this grid and the unadapted grids surrounding it. Smoothness between the nonadapted planes and the internal adapted planes was maintained by the merging process described in Ref. 15. The flow solver used this new grid to obtain the result shown in Fig. 15d. It can be seen that the flow features have sharpened considerably. The interaction of the plume shocks with the ramp and the edge flow is complex and three dimensional in nature. Experimental observations for the SERN nozzle are underway, and only limited data are currently available. Figure 16 compares the experimental shadowgraph to the computed flow along the symmetry plane downstream of the nozzle exit. Though the experimental geometry is different (it lacks the side extension for the ramp), the flow features along the symmetry plane should be the same. The experimental shadowgraph is shown in Fig. 16a and the computed Mach contours along the symmetry plane from the adapted grid are shown in Fig. 16b. The external and internal plume shocks (seen very clearly in the experimental shadowgraph) are captured well, and the agreement between the computation and the experiment is seen to be good.

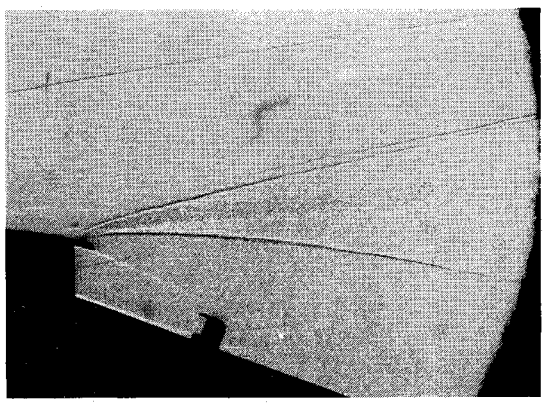

a)

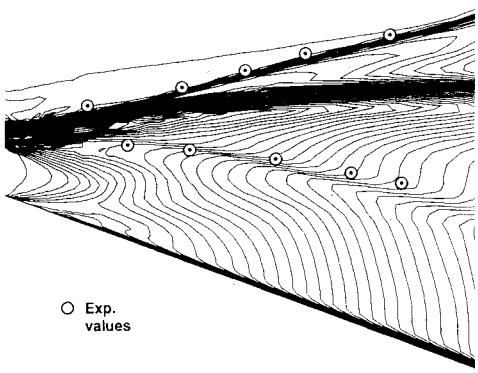

b)

Fig. 16 Flow comparison along the symmetry plane of the SERN nozzle plume flow: a) experimental shadowgraph, b) computed Mach contours, with experimental points indicated.

Conclusions

The expanded three-dimensional SAGE code has proven to be a flexible and useful tool in the solution of complex three-dimensional flow problems. The examples have shown substantially improved solutions: for the forebody of the AFE, the shock wave was considerably sharpened; for the AFE base-flow region, many flow features were resolved for the first time; for the three-dimensional ramp, the separation zone increased to more closely match that of experimental results; and for the NASP nozzle, matching grid boundaries were maintained while performing an adaption that aided in obtaining sharper flow solutions for the complex flow structures.

It should be noted that, in the given examples, grid convergence has not been established. However, we have shown the adaptive grid algorithm to be reliable and to improve the solution accuracy in all of the test cases. Although great effort has gone into simplifying user interaction, there are still several parameters that need to be carefully chosen. These parameters include the proper scalar function that defines the weight function, the relative mesh-size control, the direction and sequence of adaption, and the relationship of grid smoothness to grid alignment. It is also difficult to determine when the adaption process has provided its best possible solution. This is particularly true if no experimental data are available or if there is a lack of theoretical understanding of the flow. Another difficulty occurs if local features are important but missing in the original grid; the adaption to this solution will not result in any improvement, and only grid refinement can result in an improved solution. These are complex issues and need to be explored within the context of a specific problem.

Acknowledgments

Research support for Ethiraj Venkatapathy was provided by NASA Grant NCC2-420. The authors wish to thank Jong H. Wang of Rockwell, and Stephen Ruffin and Grant Palmer of NASA Ames Research Center for their flowfield computations both before and after the adaption process.

References

[1]Brackbill, J. U., and Saltzman, G. S., "Adaptive Zoning for Singular Problems in Two Dimensions," *Journal of Computational Physics,* Vol. 46, No. 3, 1982, pp. 342–368.

[2]Berger, M., and Oliger, J., "Adaptive Mesh Refinement for Hyperbolic Conservation Laws," *Journal of Computational Physics,* Vol. 53, No. 3, 1984, pp. 484–512.

[3]Dannenhoffer, J. F., and Baron, J. R., "Robust Grid Adaption for Complex Transonic Flows," AIAA Paper 86-0495, 1986.

[4]Thompson, J. F., "A Review on the State of the Art of Adapted Grids," AIAA Paper 84-1606, June 1984.

[5]Gnoffo, P., "A Vectorized, Finite-Volume, Adaptive Grid Algorithm Applied to Planetary Entry Flowfields," *AIAA Journal,* Vol. 21, No. 9, 1983, pp. 1249–1254.

[6]Nakahashi, K., and Deiwert, G. S., "A Practical Adaptive Grid Method for Complex Fluid Flow Problems," NASA TM-85989, June 1984.

[7]Nakahashi, K., and Deiwert, G. S., "A Three-Dimensional Adaptive Grid Method," AIAA Paper 85-0486, Jan. 1985.

[8]Nakahashi, K., and Deiwert, G. S., "A Self-Adaptive Grid Method with Application to Airfoils," AIAA Paper 85-1525, July 1985.

[9]Davies, C. B., and Venkatapathy, E., "A Simplified Self-Adaptive Grid Method, SAGE," NASA TM-102198, Oct. 1989.

[10]Venkatapathy, E., and Feiereisen, W. J., "Computational Studies of Hard-Body and 3-D Effects in Plume Flows," AIAA Paper 89-0129, 1989.

[11]Ruffin, S., and Venkatapathy, E., "Computational Design Aspects of a NASP Nozzle/Afterbody Experiment," AIAA Paper 89-0446, 1989.

[12]Klopfer, G., and Yee, H., "Viscous Hypersonic Shock-on-Shock Interaction on Blunt Cowl Lips," AIAA Paper 88-0233, Jan. 1988.

[13]Deiwert, G. S., Venkatapathy, E., Davies, C. B., Djomehri, J., and Abrahamson, K., "Application of a Self-Adaptive Grid Method to Complex Flows," NASA TM-102223, July 1989.

[14]Djomehri, J., and Deiwert, G. S., "Three-Dimensional Self-Adaptive Grid Method for Complex Flows," *Proceedings of the Second International Conference on Numerical Grid Generation in Computational Fluid Dynamics,* Miami Beach, FL, Dec. 1988.

[15]Davies, C. B., and Venkatapathy, E., "The Multidimensional Self-Adaptive Grid Code, SAGE," NASA TM-103905, 1992.

[16]Fletcher, D. G., and McDaniel, J. C., "Quantitative Characterization of a Non-Reacting, Supersonic Combustor Using Laser-Induced Iodine Fluorescence," AIAA Paper 89-2565, 1989.

[17]Palmer, G., "The Development of an Explicit Thermochemical Nonequilibrium Algorithm and its Application to Compute Three Dimensional AFE Flowfields," AIAA Paper 89-1701, 1989.

[18]Palmer, G., "Enhanced Thermochemical Nonequilibrium Computations of Flow Around the Aeroassist Flight Experiment Vehicle," AIAA Paper 90-1702, 1990.

[19]Gnoffo, P. A., "Code Calibration Program in Support of the Aeroassist Flight Experiment," *Journal of Spacecraft and Rockets,* Vol. 27, No. 2, 1990, pp. 131–142.

[20]Tam, L., and Li, C. P., "Three Dimensional Thermal and Chemical Nonequilibrium Flow Modeling for Aeroassist Flight Experiment," AIAA Paper 89-1860, 1989.

[21]Venkatapathy, E., Palmer, G., and Prabhu, D., "AFE Base Flow Computations," AIAA Paper 91-1372, June 1991.

[22]Venkatapathy, E., "Computational Results for 2-D and 3-D Ramp Flows with an Upwind Navier-Stokes Solver," *Proceedings of the Hypersonic Workshop,* Springer-Verlag (to be published).

[23]Ruffin, S. M., Venkatapathy, E., Lee, S. H., Keener, E. R., and Spaid, F. W., "Single Expansion Ramp Nozzle Simulations," AIAA Paper 92-0387, Reno, NV, Jan. 1992.